Crystalline Colloidal Array of Water Voids in Hydrogels: Direct Evidence for Entropic Trapping of Flexible Polymers

Lei Liu, Pusheng Li,[†] and Sanford A. Asher*

Contribution from the Department of Chemistry, University of Pittsburgh, Pittsburgh, Pennsylvania 15260

Received November 5, 1998

Abstract: We have developed a unique hydrogel material with a monodisperse face-centered cubic array of spherical water holes. This embedded array of holes Bragg diffracts light due to the refractive index mismatch between the holes and the interstitial gel medium. Through Bragg diffraction and absorption spectral studies, we examined the molecular weight and concentration dependence of the partitioning of linear sodium polystyrene sulfonate macromolecules between regions of different spatial constraints, i.e., the array of aqueous holes, the interstitial gel network, and the reservoir solution. We believe that our results are the first experimental verification of the phenomenon of equilibrium entropic trapping of flexible macromolecules in a polymeric gel matrix. This trapping occurs because the flexible macromolecules maximize their conformational entropy by partitioning from the gel network matrix into the embedded water holes. These mesoscopically multiphase periodic hydrogel materials may be useful for macromolecular separations in electrophoresis, filtration, and chromatography.

Introduction

The partitioning of a flexible polymer chain between different volume elements of a porous medium is important in areas such as size exclusion chromatography, gel electrophoresis, filtration, membrane separation, etc. Although intrinsically a thermodynamic phenomenon, such partitioning often plays an important role in many dynamic processes, such as diffusion and electrophoretic migration of polymer chains through porous media.[1−9]

In the absence of specific interactions between the polymer chains and the media, it has been suggested that the volume-constrained chain conformational entropy controls the partitioning of flexible polymer chains between regions of different volumes.[10−18] Figure 1 illustrates a polymeric gel system where the average network matrix provides only narrow channels where the polymer chain must be elongated; the polymer chain is constrained with only limited conformational possibilities. In contrast, if the polymer chain occupied a large spherical void, it would be able to adopt all of its possible conformations and would possess a larger conformational entropy. Consequently, the polymer chain should preferentially partition into this large void. From a dynamic point of view, if the polymer chain tries to leave the void, it encounters an entropic barrier since its conformations must be restricted to those which can squeeze into the narrow channels. Thus, large voids in a porous medium have been proposed to function as "entropic traps" to retard the diffusion and transportation of flexible polymer chains.

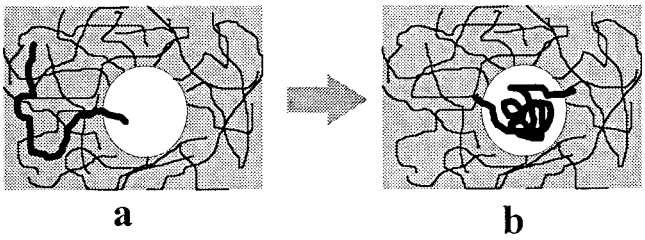

Figure 1. Illustration of entropic trapping phenomenon. A flexible chain macromolecule is (a) elongated in a region of high spatial constraints and (b) relaxed and folded in a region of low spatial constraints.

Evidence for this entropic trapping phenomenon has come from experimental studies on diffusion or low-field electrophoretic migration of flexible chain polymers in various types of porous media, such as entangled solutions,[1,2] cross-linked polymeric gel networks,[3−8] and model membranes of well-controlled pores.[9] It was observed that, when the equilibrium dimension of the macromolecules was comparable to the mean pore size of the medium and the electric field was weak, the

* To whom correspondence should be sent. Phone: (412) 624-8570. Fax: (412) 624-0588. E-mail: asher+@pitt.edu.

[†]Current address: Epsilon Inc., HPOS, 50 Cambridge St., Burlington, MA 01803.

(1) Nemoto, N.; Kishine, M.; Inoue, T.; Osaki, K. *Macromolecules* **1990**, *23*, 659−664.
(2) Kim, H.; Chang, T.; Yohanan, J. M.; Wang, L.; Yu, H. *Macromolecules* **1986**, *19*, 2737−2744.
(3) Smisek, D. L.; Hoagland, D. A. *Science* **1990**, *248*, 1221−1223.
(4) Arvanitidou, E.; Hoagland, D. *Phys. Rev. Lett.* **1991**, *67*, 1464−1466.
(5) Lodge, T. P.; Rotstein, N. A. *Macromolecules* **1992**, *25*, 1316−1325.
(6) Muthukumar, M.; Hoagland, D. A. *Macromolecules* **1992**, *25*, 6696−6698.
(7) Mayer, P.; Slater, G. W.; Drouin, G. *Appl. Theor. Electrophor.* **1993**, *3*, 147−155.
(8) Rousseau, J.; Drouin, G.; Slater, G. W. *Phys. Rev. Lett.* **1997**, *79*, 1945−1948.
(9) Guillot, G.; Léger, L.; Rondelez, F. *Macromolecules* **1985**, *18*, 2531−2537.
(10) Baumgartner, A.; Muthukumar, M. *J. Chem. Phys.* **1987**, *87*, 3082−3088.
(11) Muthukumar, M.; Baumgartner, A. *Macromolecules* **1989**, *22*, 1937−1941.
(12) Muthukumar, M.; Baumgartner, A. *Macromolecules* **1989**, *22*, 1941−1946.
(13) Casassa, E. F. *Polym. Lett.* **1967**, *5*, 773−778.
(14) Casassa, E. F.; Tagami, Y. *Macromolecules* **1969**, *2*, 14−26.
(15) Noolandi, J.; Rousseau, J.; Slater, G. W. *Phys. Rev. Lett.* **1987**, *58*, 2428−2431.
(16) Slater, G. W.; Wu, S. Y. *Phys. Rev. Lett.* **1995**, *75*, 164−167.
(17) Daoud, M.; de Gennes, P. G. *J. Phys. (Les Ulis, Fr.)* **1977**, *38*, 85−93.
(18) Brochard, F.; de Gennes, P. G. *J. Chem. Phys.* **1977**, *67*, 52−56.

10.1021/ja983843n CCC: $18.00
Published on Web 04/09/1999

diffusion constant (D) and electrophoretic mobility (μ) depended more strongly on molecular weight than predicted by either Ogsten sieving or a reptation model. This behavior was rationalized by an entropic barrier transport model which was first formally proposed by Muthukumar and Baumgartner.[10−12]

Casassa[13,14] was the first to calculate, from ideal random walk statistics of chain conformational entropy, the equilibrium partition coefficients of a single polymer chain between confining volumes of different shapes (i.e., spherical, cylindrical, slab-shaped, etc.). Utilizing the scaling argument for polymer solutions,[20] Daoud and de Gennes,[17] Brochard and de Gennes,[18] and Daoudi and Brochard[19] investigated both the partitioning and the transport properties of self-avoiding polymer chains in good solvents in small cylindrical tubes as a function of concentration, ranging from the dilute solution regime to the entanglement regime.

The dynamics of both non-self-avoiding and self-avoiding polymer chains in various two-dimensional or three-dimensional model porous media have been studied by formalisms such as Monte Carlo methods,[10−12] biased reptation model,[15,22] Brownian dynamics,[23] bond fluctuation algorithms,[21] etc.[16,24−27] All theoretical attempts so far assume model pores or obstacles with well-defined boundary conditions, such as a cubic array of square boxes connected by narrow channels,[11] a two-dimensional lattice with random obstacles,[10,12,16] "straits and lakes",[22] an infinitely long tube with a periodically oscillating width,[23] etc.[15,24−27]

However, the relevance of any of these approaches to polymer diffusion in a swollen polymeric gel matrix remains unclear. As far as we know, except for the work described here,[28] no measurements have been made of the equilibrium partitioning of a flexible chain polymer in a swollen polymeric gel matrix. Quantitative comparisons of theoretical and experimental results have been difficult due to the lack of a well-defined pore size, polydispersity, and morphology in typical gel matrices.

In this report, we give the first direct evidence for equilibrium entropic trapping phenomena in swollen polymeric gel media by utilizing polymerized crystalline colloidal array (PCCA) materials.[28−37] Crystalline colloidal arrays (CCAs) are three-dimensional periodic arrays formed by the self-assembly of monodisperse macroionic colloidal spheres in low ionic strength aqueous solutions.[29−38] This self-assembly minimizes the total interparticle electrostatic repulsive energy of the system. CCAs adopt either a body-centered cubic (bcc) or a face-centered cubic (fcc) structure and orient with their highest particle density lattice planes (i.e., bcc (110) or fcc (111) planes) parallel to the container walls.[30−32] Similar to atomic crystals diffracting X-rays, CCAs strongly Bragg diffract light in the near-IR through UV spectral regions.[31−38] We have previously developed quantitative models of the dependence of the Bragg diffraction on the CCA structure and optical constants.[38]

For this study, we developed[28] a new material where a CCA of water-filled spherical voids occurs in a cross-linked polyacrylamide hydrogel network (vide infra). Bragg diffraction from this PCCA of water voids is used to sensitively probe the solution refractive index changes. The intensity of the Bragg diffraction is an in situ monitor of the difference in polymer concentrations between the polyacrylamide gel and the water spheres. We determine the equilibrium partition coefficients of a linear polymer (sodium polystyrene sulfonate, NaPSS) between regions of different spatial constraints. We have determined the dependence of these partition coefficients on the polymer concentration and molecular weight.

Experimental Section

1. Materials and Instrumentation. Monodisperse colloidal silica spheres were obtained from Nissan Chemical Industries, Ltd. (PST-1), as a ca. 20% (by weight) aqueous suspension (pH, 8−10) with a particle diameter of 101 ± 6 nm, as determined by transmission electron microscopy. The ionic impurities in the suspension were removed by exposure of the solution to mixed-bed ion-exchange resin (Bio-Rad Laboratories, AG 501-X8, 20−50 mesh). Acrylamide (AMD, Polysciences, Inc.), *N*,*N*′-methylene-bisacrylamide (bis-AMD, Fluka Chemical Corp.), and photoinitiator 2,2-diethoxyacetophenone (DEAP, Aldrich) were used directly without further purification. Narrow distribution molecular weight standards of sodium polystyrene sulfonate (NaPSS, $M_w/M_n \approx 1.10$) were purchased from Scientific Polymer Products, Inc., and Polysciences, Inc. The molecular weights quoted are the weight-average molecular weights (M_w). A Bausch & Lomb refractometer was used to measure the NaPSS solution refractive indices. A Perkin-Elmer Lambda 9 UV/VIS/NIR spectrophotometer was used to measure the NaPSS absorption spectra and to monitor the diffraction from the CCA.

2. Fabrication of a Polymerized CCA of Spherical Holes. Figure 2 illustrates the fabrication of a PCCA of spherical holes (HPCCA). A suspension of ∼101-nm-diameter monodisperse silica spheres was allowed to self-assemble into a CCA by removing the ionic impurities with ion-exchange resin. After ion-exchange, we observed strong iridescence from the silica CCA suspension. The diffracted wavelength was controlled by varying the CCA lattice interplanar spacing, which could be continuously adjusted by varying the number density of silica spheres in the dispersion.

We immobilized the CCA structure by polymerizing a cross-linked hydrogel network around the sphere array (PCCA). This methodology has also been described in detail elsewhere.[33−37] Here we mixed the silica CCA aqueous suspension with the monomer AMD, the cross-linker bis-AMD, and the photoinitiator DEAP. The mixture was then injected between two quartz plates separated by a ∼100-μm-thick spacer and exposed to UV light by using a mercury lamp. The acrylamide gel polymerization resulted in a cross-linked hydrogel film, where the silica CCA was permanently locked in position. A typical prepolymerization mixture would contain a silica CCA suspension, 20% (w/w) total monomer (AMD + bis-AMD) with a 9:1 AMD-to-bis-AMD ratio, and 0.1% (w/w) DEAP. The final volume fraction of the silica spheres in the mixture is about 7%.

(19) Daoudi, S.; Brochard, F. *Macromolecules* **1978**, *11*, 751−758.
(20) De Gennes, P. G. *Scaling Concepts in Polymer Physics*; Cornell University Press: Ithaca, NY, 1979.
(21) Carmesin, I.; Kremer, K. *Macromolecules* **1988**, *21*, 2819−2823.
(22) Zimm, B. H. *Phys. Rev. Lett.* **1988**, *61*, 2965−2968.
(23) Nixon, G. I.; Slater, G. W. *Phys. Rev. E* **1996**, *53*, 4969−4980.
(24) Volkmuth, W. D.; Duke, T.; Wu, M. C.; Austin, R. H. *Phys. Rev. Lett.* **1994**, *72*, 2117−2120.
(25) Slater, G. W.; Guo, H. L.; Nixon, G. I. *Phys. Rev. Lett.* **1997**, *78*, 1170−1173.
(26) Zwanzig, R. *J. Phys. Chem.* **1992**, *96*, 3926−3930.
(27) Sheu, W.-S.; Yang, D.-Y.; Sheu, S.-Y. *J. Chem. Phys.* **1997**, *106*, 9050−9056.
(28) Liu, L.; Li, P.; Asher, S. A. *Nature* **1998**, *397*, 141−144.
(29) Hiltner, P. A.; Krieger, I. M. *J. Phys. Chem.* **1969**, *73*, 2386-2389.
(30) Davis, K. E.; Russel, W. B.; Glantschnig, W. J. *Science* **1989**, *245*, 507−510.
(31) Monovoukas, Y.; Gast, A. P. *Langmuir* **1991**, *7*, 460−468.
(32) Kesavamoorthy, R.; Tandon, S.; Xu, S.; Jagannathan, S.; Asher, S. A. *J. Colloid Interface Sci.* **1992**, *153*, 188−198.
(33) Clark, N. A.; Hurd, A. J.; Ackerson, B. J. *Nature* **1979**, *281*, 57−60.
(34) Asher, S. A.; Jagannathan, S. U.S. Patent 5,281,370, 1994.
(35) Asher, S. A.; Holtz, J.; Liu, L.; Wu, Z. *J. Am. Chem. Soc.* **1994**, *116*, 4997−4998.
(36) Weissman, J. M.; Sunkara, H. B.; Tse, A. S.; Asher, S. A. *Science* **1996**, *274*, 959−960.
(37) Pan, G.; Kesavamoorthy, R.; Asher, S. A. *Phys. Rev. Lett.* **1997**, *78*, 3860−3863.
(38) Rundquist, P. A.; Photinos, P.; Jagannathan, S.; Asher, S. A. *J. Chem. Phys.* **1989**, *91*, 4932−4941.

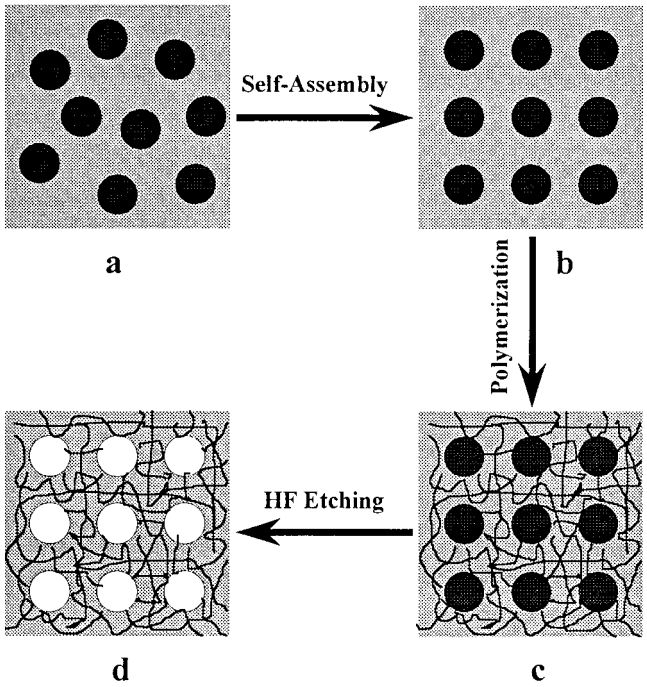

Figure 2. Fabrication of a cubic array of spherical water holes. (a) Random silica colloid aqueous suspension, (b) self-assembled crystalline colloidal array (CCA) in deionized water, (c) polyacrylamide hydrogel film embedded with silica CCA (PCCA), and (d) polyacrylamide hydrogel of CCA of holes (HPCCA).

Due to the high polymer content and high cross-linker density, the resulting PCCA films were sufficiently robust to allow further chemical modification. We soaked the films in a 10% (w/w) hydrofluoric acid solution for about 5 min to etch out the silica colloids. After careful washing with deionized water, a HPCCA of ~100-nm-diameter water-filled spherical holes was created. Both diffraction (vide infra) and gravimetric analysis showed that the silica was completely removed and that the etching had little effect on the hydrogel network.

3. Dependence of HPCCA Diffraction on Chemical Composition. The intensity and wavelength of light Bragg diffracted by the array of water holes in the HPCCA depend on the refractive indices of the scattering entities (n_{hole}), the interstitial gel medium (n_{medium}), and the overall crystal ($n_{crystal}$). These refractive indices in turn depend on their corresponding chemical compositions. Therefore, by analyzing the diffraction profile changes, we can sensitively probe these refractive index changes. We will use this approach to monitor the NaPSS polymer concentrations in the HPCCA medium and holes.

The following expressions relate the refractive indices of these regions to the local NaPSS solution concentrations:

$$n_{hole} = n_{water}(1 - C_H) + n_{PSS}C_H \quad (1)$$

$$n_{medium} = n_{AMD}\phi_a + (1 - \phi_a)[n_{water}(1 - C_G) + n_{PSS}C_G] \quad (2)$$

$$n_{crystal} = n_{medium}(1 - \phi_{hole}) + n_{hole}\phi_{hole} \quad (3)$$

where n_{water} and n_{AMD} represents the refractive indices of water and AMD, C_H is the NaPSS weight percent concentration in the holes, C_G is the NaPSS weight percent concentration in the hydrogel medium with respect to the solution mass only (i.e., not including the mass of polyacrylamide network), ϕ_{hole} is the volume fraction of the holes in the whole system, and ϕ_a is the volume fraction of the polyacrylamide network in the gel medium. Figure 3 demonstrates that, in the concentration range used here, the refractive index of the NaPSS solution is linearly proportional to its weight percent concentration. Therefore, n_{PSS} represents the "apparent" value of the NaPSS refractive index, which is calculated from the slope to be 1.5065.

The CCA diffracted intensity and wavelength can be calculated by using a model which combines dynamical X-ray diffraction theory and particle light-scattering theory.[38−41] The relative diffraction intensity

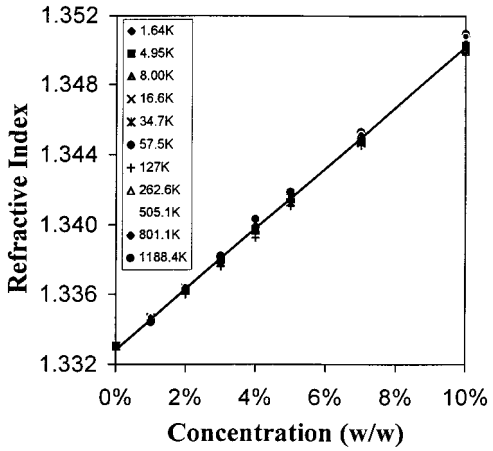

Figure 3. Concentration dependence of the NaPSS solution refractive index for all NaPSS molecular weight standards. The legend indicates the NaPSS molecular weight, where K = 1000 Da.

is calculated as the ratio of the diffracted power (P_d) to the incident power (P_0) for a perfect nonabsorbing crystal:

$$\frac{P_d}{P_0} = \frac{1}{y^2 + (y^2 - 1)\cot^2(A\sqrt{y^2 - 1})} \quad \text{if } y > 1$$

$$\frac{P_d}{P_0} = \frac{1}{y^2 + (1 - y^2)\coth^2(A\sqrt{1 - y^2})} \quad \text{if } y < 1 \quad (4)$$

$$\frac{P_d}{P_0} = \frac{A^2}{A^2 + 1} \quad \text{if } y = 1$$

The measured extinction (E) is defined as

$$E = -\log T = -\log\left(1 - \frac{P_d}{P_0}\right) \quad (5)$$

where T is the transmittance.

Assuming diffraction from BCC (110) lattice planes for light at normal incidence,

$$y = \frac{\Psi_0 - 2[(\lambda - \lambda^B)/\lambda^B]}{|\Psi_H|} \quad (6)$$

$$\lambda^B = 2n_{crystal}d_{110} \quad (7)$$

$$A = \frac{\pi n_{crystal}t_0|\Psi_H|}{\lambda^B} \quad (8)$$

$$\Psi_0 = \left(\frac{n_{crystal}}{n_{medium}}\right)^2 - 1 \quad (9)$$

$$\Psi_H = \frac{1}{2\sqrt{2}\pi^2}\left[\frac{3(m^2 - 1)}{m^2 + 2}\right](\sin u - u\cos u) \quad (10)$$

$$u = \frac{2\pi n_{crystal}D_0}{\lambda^B} \quad (11)$$

where λ^B is the kinematic Bragg diffraction wavelength in air, d_{110} is the interplanar spacing of the (110) lattice plane, t_0 is the crystal thickness, $m = n_{hole}/n_{medium}$, and D_0 is the particle diameter.

(39) Liu, L.; Li, P.; Asher, S. A. *J. Am. Chem. Soc.* **1997**, *119*, 2729−2732.

(40) Zachariasen, W. H. *Theory of X-ray Diffraction in Crystals*; John Wiley and Sons: New York, NY, 1946.

(41) Van Hulst, H. C. *Light Scattering by Small Particles*; John Wiley and Sons: New York, NY, 1957.

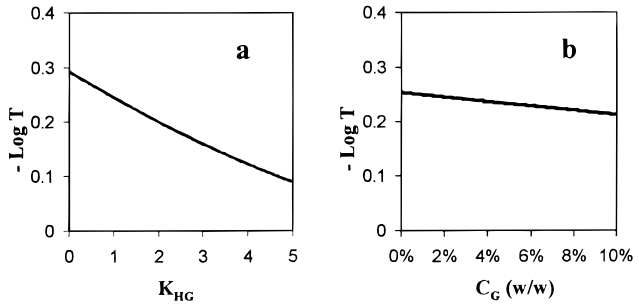

Figure 4. Calculated diffraction change as a function of the partition coefficient K_{HG} and the NaPSS concentration C_G. (a) Extinction vs K_{HG} when $C_G = 2\%$ (w/w). (b) Extinction vs C_G when $K_{HG} = 1$.

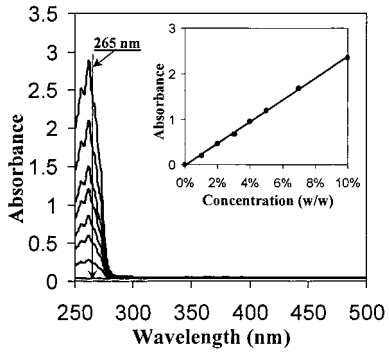

Figure 5. Absorption spectra of PSS aqueous solutions at concentrations of 10, 7, 5, 4, 3, 2, 1, and 0 wt %. The inset shows the linear correlation between the 265-nm absorbance and concentration.

If the hydrogel volume is constant, changes in the diffraction profile will derive only from the refractive index changes. In this case, the diffraction extinction is governed by the refractive index difference between the medium (n_{medium}) and the scatterers (n_{hole}), while the diffracted wavelength is governed by the overall crystal refractive index ($n_{crystal}$).

Figure 4 shows the calculated dependence of the diffraction extinction on C_G and the partition coefficient between the holes and the gel medium, $K_{HG} = C_H/C_G$. The diffraction extinction strongly depends on K_{HG} because K_{HG} diminishes the refractive index mismatch between the holes and the medium. If $K_{HG} = 1$ (no partitioning), the diffraction extinction only slightly decreases as C_G increases.

4. Determination of C_G from NaPSS Absorption. Assuming that the partitioning of the NaPSS polymer chains from the reservoir solution into the porous hydrogel medium is identical in the presence or absence of the CCA, we can independently determine C_G by absorption spectroscopy. We made 200-μm-thick blank hydrogel films with the same composition as that of the PCCA but without the silica CCA. We then measured the absorption spectra of the blank hydrogel film in water and in NaPSS solutions of different concentrations and molecular weights. Difference absorption spectra were used to minimize the total background contributions from the scattering and absorption of the hydrogel network.

Figure 5 shows the concentration dependence of the NaPSS absorption and a typical calibration curve at 265 nm. The calibration curves are linear over the entire concentration range studied. By comparing the NaPSS absorption in the gel media and in the reservoir solution, we obtained C_G values for each particular molecular weight and reservoir concentration.

5. Determination of C_H and K_{HG}. Although the hydrogel films used in these studies were highly cross-linked and rigid, they still slightly changed volume for different NaPSS concentrations. This gel volume change is an important issue since it alters the HPCCA lattice parameters and the size of the holes. Consequently, the overall change in the diffraction profiles will contain the contributions not only from refractive index changes but also from gel volume changes.

We parametrized eqs 1−11 with the gel swelling ratio (r), defined as the ratio of the gel volume soaked in a particular NaPSS solution over that in pure water. Assuming a homogeneous change throughout the hydrogel, the parameters D_0, d_{110}, t_0, and ϕ_a used in eqs 1−11 will change to $r^{1/3}D_0$, $r^{1/3}d_{110}$, $r^{1/3}t_0$, and $r^{-1}\phi_a$, respectively. Since C_G is determined from the absorption measurements, we have two observables, the extinction E and the diffracted wavelength λ, which depend on only two variables, the concentration C_H (or the partition coefficient K_{HG}) and the swelling ratio r. Therefore, we can determine C_H and r directly from the diffraction data.

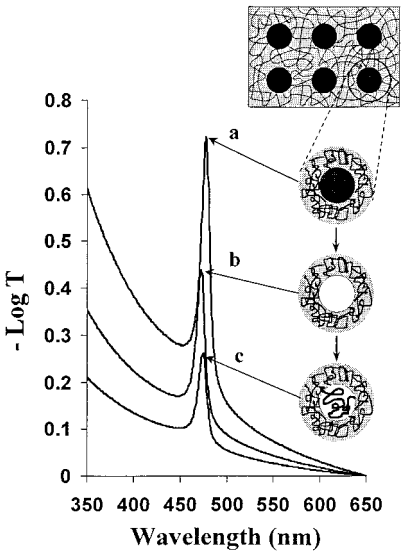

Figure 6. Diffraction spectra of (a) silica sphere PCCA, (b) HPCCA, and (c) NaPSS-filled HPCCA.

Experimentally, we first measured the diffraction spectra of the HPCCA in pure water. We then soaked the HPCCA in a NaPSS solution of a particular concentration and molecular weight for 3 days, after which we remeasured the diffraction. The surrounding reservoir was essentially infinitely larger than the gel films (~100-μm-thick disks, ~8 mm in diameter). Thus, the NaPSS concentration in the reservoir stayed constant. The soaking time was chosen sufficiently long that equilibrium occurred; no further diffraction changes were observed. In addition, we utilized a single HPCCA film throughout this study to minimize variations and errors.

Figure 6 shows the observed diffraction spectra for different PCCA compositions. The changes in the diffraction extinction and wavelength reflect basically the refractive index changes. As the silica spheres are removed by HF etching (a → b), the PCCA diffraction extinction decreases because the refractive index mismatch between the water and gel medium is smaller than that between the silica and the gel medium. The diffraction also slightly blue-shifts because $n_{crystal}$ has decreased. As the HPCCA is soaked in the NaPSS solution (b → c), the diffraction extinction further decreases since the mismatch between n_{medium} and n_{hole} is further reduced. The slight increase in $n_{crystal}$ should red-shift the diffracted wavelength. However, the magnitude of this shift will be comparable to that which would occur from gel volume changes.

To systematically measure the diffraction extinction and wavelength, we curve-fit each of the diffraction spectra (Figure 7). A perfect CCA will show a sharp symmetric diffraction peak. However, crystal imperfections and incident beam divergence will result in an asymmetry on the shorter wavelength side. Furthermore, the scattering from defects and the absorption of NaPSS and polyacrylamide give a background which increases as the wavelength decreases.

We used a Lorentzian band shape (Figure 7, line 2) to model the ideal crystal diffraction and a log-normal peak (line 4) to model the asymmetry. We used a single Gaussian (line 3) with its maximum in the UV region to model the increasing background. Furthermore, a baseline offset (line 5) was used to account for interface reflections.

We also independently measured the r values by monitoring the gel disk diameter changes using a magnifier with a contact reticle. The results agree well with those calculated from the diffraction analysis; the hydrogel linear dimension changes are all less than 1%. This

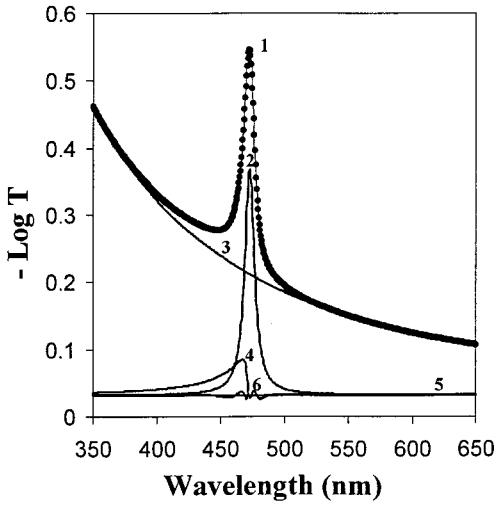

Figure 7. Curve-fitting of PCCA diffraction profile. (1) The dotted line is an experimental spectrum, and the thin line is the overall curve fit (2) Lorentzian fit for perfect crystal diffraction. (3) Gaussian fit for absorption and random scattering. (4) Log-normal fit for crystal defects and lattice plane misalignment. (5) Baseline offset. (6) Curve-fitting residual.

agreement reinforces the reliability we can expect for the methodology used in this study.

Results

When the HPCCA film is exposed to the NaPSS reservoir, the NaPSS partitions among the three regions of different spatial constraints (Figure 8A). The region of the holes consists of the monodisperse spherical aqueous cavities created by etching out the silica spheres. These spherical holes (presumably the same diameter as the original silica colloids (∼101 nm)) occur in a cubic array lattice. The second region consists of the interstitial hydrogel space, which is a randomly interwoven network of cross-linked polyacrylamide chains which form pores of different sizes (vide infra). This broad distribution of pores has an average diameter of several nanometers.[42] The third region is the infinite NaPSS solution reservoir, which has no external constraints except excluded volume and polymer entanglements (vide infra).

Each experiment utilizes a NaPSS polymer of a defined molecular weight. C_H, C_G, and C_S represent the NaPSS weight percent in the holes, the gel, and the reservoir, respectively. Note that C_G is normalized to the available volume of the gel; i.e., the polyacrylamide chain volume is subtracted. We define the partition coefficients (the concentration ratios) among the three regions as K_{HG}, K_{SG}, and K_{SH} (Figure 8A).

1. Molecular Weight Dependence of the Partition Coefficients. Figure 8B shows the dependence of the NaPSS partition coefficients on molecular weight at various reservoir concentrations (C_S). While the NaPSS molecular weight increases, the partition coefficients increase, and at the highest molecular weight, $K_{HG} \approx 4$ and $K_{SG} \approx 6$. This partitioning behavior is the first direct evidence of the entropic trapping phenomenon.

Figure 8B shows that ln K_{HG} and ln K_{SG} initially increase rapidly and almost linearly with molecular weight and then level off at higher molecular weights. Ln K_{SH} linearly increases in the entire molecular weight range but with a smaller slope than that of ln K_{HG} or ln K_{SG}. This linear relationship between ln K and molecular weight is expected from entropic trapping theory, where the entropy term is proportional to the molecular weight (vide infra).

At the lowest molecular weight, we observe that the partition coefficients are sometimes less than 1, and ln K is negative. This indicates that an increase of NaPSS concentration occurs in the polyacrylamide network region; entropic trapping effects become insignificant for low-molecular-weight polymers, and some affinity may exist between NaPSS and polyacrylamide network.

2. Concentration Dependence of the Partition Coefficients. Figure 8C shows the NaPSS concentration dependence of the partition coefficients for different molecular weights. K_{HG} shows a concentration dependence similar to that of K_{SG}. At low molecular weights, K_{HG} and K_{SG} only slightly increase as C_S increases. In contrast, at high molecular weights, they both sharply increase with C_S until they reach a maximum at ∼5%C_S and then decrease as C_S further increases. In contrast, the dependence of K_{SH} on C_S appears very different. K_{SH} increases monotonically with C_S (Figure 8C), with a slight leveling-off for the highest molecular weights. Figure 8C also shows that the partition coefficients rise more sharply with concentration for higher molecular weights. This indicates a larger concentration dependence of entropic trapping for higher molecular weights.

Discussion

The partition coefficients strongly depend on the NaPSS molecular weight. This must result from an entropy effect since any enthalpic interactions between NaPSS chains or NaPSS and hydrogel network should have little molecular weight dependence. In addition, the embedded holes essentially possess the same chemical properties as the rest of gel medium except that the average pore sizes are different. The dissolved NaPSS chains should possess the same enthalpy in the gel medium and in the holes. Thus, the partitioning observed here must result predominately from the polymer chain conformational entropy differences due to the different spatial constraints.

Electrostatic effects due to the NaPSS polyelectrolyte properties should not play a significant role in this partitioning process, for the following reasons: (1) There are no specific electrostatic interactions between NaPSS and the polyacrylamide chains. (2) The inter- or intramolecular interactions of NaPSS should be the same in the gel and in the holes. (3) The electrostatic effects on the NaPSS conformation should be charge density dependent and thus not strongly molecular weight dependent. (4) We studied the partitioning of NaCl in the same concentration range as for NaPSS. No significant partitioning was observed for NaCl, which indicates that simple electrolytes do not selectively partition between the gel and the holes.

The configuration of a flexible polymer chain can be treated using random walk statistics. When a polymer chain is confined to a box with an infinitely high potential energy barrier, the number of possible configurations becomes limited compared to that in free space. Thus, in the box, the polymer chain possesses less conformational entropy. The smaller the box, the less conformational freedom. Consequently, a polymer chain will preferentially partition into the largest box with the least spatial constraints.

A few groups have calculated the conformational entropy and the expected partitioning for a flexible polymer chain in confined spaces of particular sizes and shapes.[11−14,17−20] These results can be generalized by the following scaling arguments. The partition coefficient, K_{ij}, of a flexible polymer chain between

(42) Righetti, P. G. *J. Chromatogr. A* **1995**, *698*, 3−17.

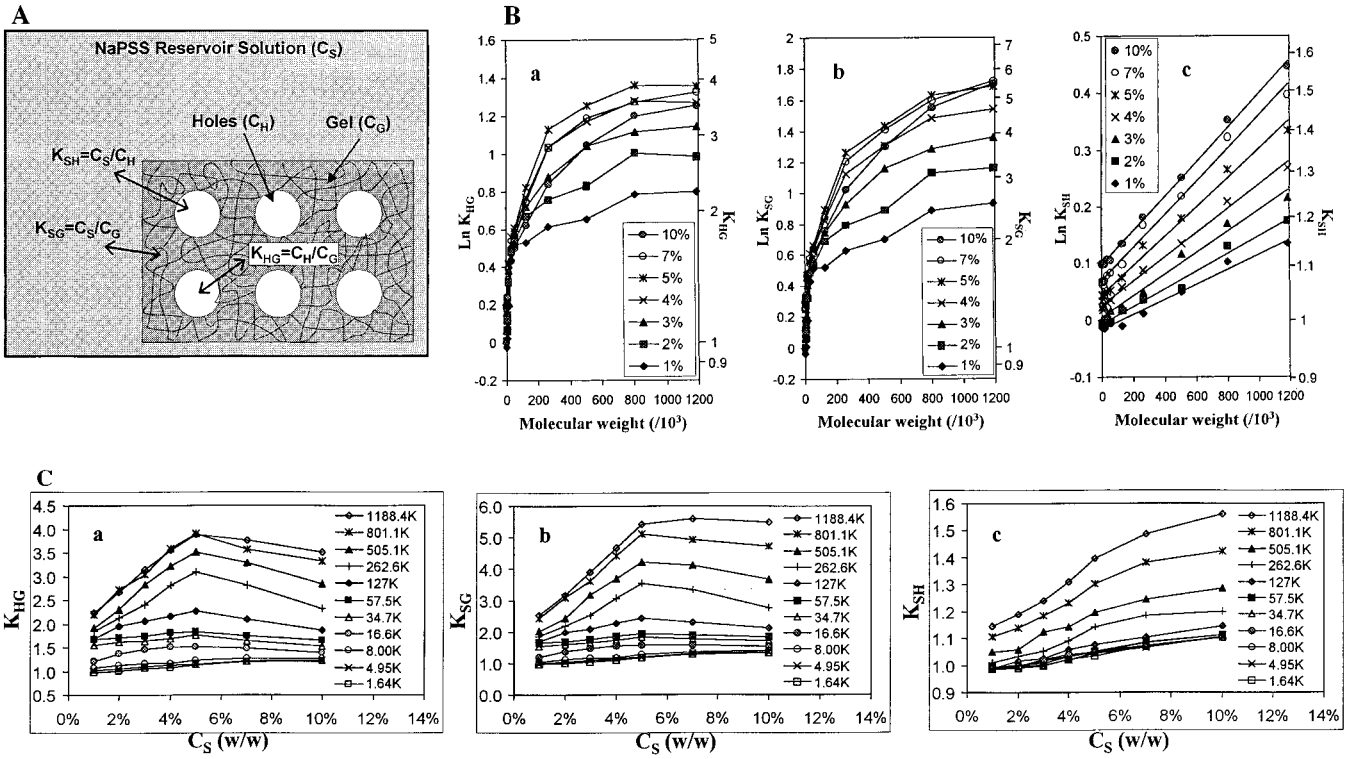

Figure 8. (A) Schematic of NaPSS partitioning among the three regions: the holes, the gel, and the reservoir. C_H, C_G, and C_S are the NaPSS weight percent concentrations in the corresponding regions. (B) Molecular weight dependence of the partition coefficients of NaPSS among the three regions. The different symbols denote the weight percentage of NaPSS in the reservoir solution. The curves connecting the points in panels a and b are used to guide the eye, while the lines in panel c are the linear least-squares fits. (C) Concentration dependence of the partition coefficients of NaPSS among the three regions. The different symbols indicate the different NaPSS molecular weights. The lines through the data are used to guide the eye.

two cavities i and j of different sizes is

$$K_{ij} \equiv \frac{C_i}{C_j} \sim \exp\left(-\frac{\Delta G_{ij}}{k_B T}\right) \tag{12}$$

$$\Delta G_{ij} \equiv G_i - G_j \tag{13}$$

where C_i and C_j are the concentrations in cavities i and j, respectively, and G_i and G_j are the corresponding Gibbs free energies.

For an entropy-dominated partitioning, where the enthalpy differences are negligible, the total free energy for a Gaussian chain at constant temperature scales as[11−14,17−20]

$$G_i \sim \left(\frac{R_G}{R_i}\right)^2 \sim N\left(\frac{a}{R_i}\right)^2 \tag{14a}$$

or

$$G_i \sim \left(\frac{R_G}{R_i}\right)^{1/\upsilon} \sim N\left(\frac{a}{R_i}\right)^{5/3} \tag{14b}$$

where N is the number of segments (steps of the random walk) for a polymer chain, a is the Kuhn step length, υ is the Flory universal exponent, which is equal to 3/5 for self-avoiding chains,[20,42] R_G is the radius of gyration for the polymer chain, and R_i is the characteristic radius of the ith cavity. G_i is defined with respect to the reference state where R_i = infinity.

Equation 14a treats an ideal random flight chain, while eq 14b includes self-excluded volume effects. These simple predictions are valid only for well-defined rigid boundary conditions, where the cavities are sufficiently large to accommodate the entire polymer chain. As the authors pointed out, they may not be applicable, and certainly are not quantitative, for the case of a swollen polymeric hydrogel system.

The actual hydrogel matrix is extremely complex without well-defined boundaries. For the ∼20% (v/v) hydrogel used here, the matrix would most likely consist of a dense net of cross-linked acrylamide polymers woven through the solution. This net acts as an excluded volume which limits the available conformations of the polymer chains. For the hydrogel here and for the highest polymer molecular weight, we can use the observed partition coefficients to calculate a "trapping entropy" of $\Delta S \approx 2.8$ cal mol^{-1} K^{-1} between the gel and the water pockets, and $\Delta S \approx 3.4$ cal mol^{-1} K^{-1} between the gel and the solution reservoir.

1. Molecular Weight Dependence of the Partition Coefficients. In the entropic trapping regime, statistical thermodynamics predicts that the partition coefficient from a smaller cavity to a larger one will increase with polymer molecular weight and the size difference between the two cavities, since the constrained conformational entropy scales with the polymer chain length and inversely with the size of the confining volume (eqs 12−14b). These predictions qualitatively agree with the results presented in Figure 8B. The partition coefficient values occur in the order $K_{SG} > K_{HG} \gg K_{SH}$.

However, the theory further predicts that the logarithm of the partition coefficients should increase linearly with the molecular weight. Figure 8B shows that ln K_{SH} vs molecular weight (8B-c) follows this prediction, while ln K_{HG} (8B-a) and ln K_{SG} (8B-b) show approximately linear behavior only for low molecular weights but level off as the molecular weight further increases. Careful examination shows that ln K_{HG} and ln K_{SG} increase almost linearly with ln N. This indicates that ln K_{HG}

and ln K_{SG} appear to increase with a fractional power of molecular weight, i.e., ln K_{HG} or ln $K_{SG} \sim N^{1-\alpha}$, where $0 < \alpha < 1$.

Since the chain conformational entropy must scale with polymer molecular weight, this result suggests that the effective size of the cross-linked hydrogel confining space depends on molecular weight. In contrast, the theory assumes single-sized cavities and well-defined rigid boundaries, and that each cavity is large enough to contain the entire polymer chain. Thus, these conditions are not fulfilled here. In the hydrogel matrix, the water forms a continuous phase which is interwoven three-dimensionally with the cross-linked polyacrylamide chains. The boundaries of the "cavities" in the hydrogel matrix are poorly defined.

Our studies utilize a broad range of NaPSS molecular weights from 1.64×10^3 to 1.2×10^6 Da, whose radii of gyration ranges from a few nanometers to about 30 nm.[9] In comparison, the average cavity size of a hydrogel matrix is expected to be about several nanometers to 10 nm, depending on the polymer and cross-linker content.[41] When a NaPSS molecule is too large to be contained in a single cavity, it will simultaneously occupy two or many adjacent cavities. Each section will behave like an independent polymer of smaller molecular weight. This effect will decrease the molecular weight dependence of entropic trapping. A similar case was examined using Monte Carlo simulations by Muthukumar and Baumgartner, who reported that the constrained polymer conformational entropy became weakly dependent, or could even become independent of molecular weight, if the polymer molecule simultaneously occupied two or more square boxes connected by short bottleneck channels.[11,12]

Thus, the effective size of the hydrogel matrix confining space is likely to be molecular weight dependent: the larger the polymer chain, the larger the space required. We can modify eq 14 such that the size of the constraining space will increase with the polymer molecular weight, i.e., $R_i \sim N^{\alpha v}$, where $0 < \alpha < 1$. This will decrease the molecular weight dependence of the conformational entropy and decrease the slope of ln K, i.e., ln $K \sim G_i \sim N^{1-\alpha}$.

The random, large pore size distribution of the hydrogel matrix also complicates our comparison to theory, since our partition coefficients are related to the statistical average of the constrained entropy over all cavity sizes, which, as stated above, are molecular weight dependent. For low-molecular-weight polymer chains, almost all of the cavities are large enough to contain the whole chain; therefore, ln K values should be a linear function of the molecular weight. However, for higher molecular weight chains, especially those which are much larger than the average pore dimension of the hydrogel medium, only a fraction of the cavities are large enough to contain the whole polymer chain and contribute to the linear relationship.

For the lowest molecular weights, we observe partition coefficients less than unity, which we attribute to a weak affinity between the NaPSS polymer and the polyacrylamide network. This effect is more pronounced where the gel network density is higher and could be relatively significant when the entropic trapping effect is small.

2. Concentration Dependence of the Partition Coefficients. The notable increase of the partition coefficients with concentration for the high-molecular-weight polymers is surprising and is not predicated, as far as we know. We speculate that our observed concentration dependence of the partition coefficients results from the size distribution of the acrylamide hydrogel pores. The low polymer molecular weights access the small and large gel pores similarly. Thus, little concentration dependence is observed for the partition coefficients. However, at high molecular weights and low polymer concentrations, the polymer molecules partition preferentially into the largest acrylamide gel pores. For example, R_G for a molecular weight of 1.1×10^6 Da is ~30 nm, while for a molecular weight of $\sim 1 \times 10^5$ Da, R_G is ~10 nm. A concentration increase for the high-molecular-weight polymer requires that the incremental polymer chains localize into smaller gel pores, which show increased partition coefficients into the holes and the solution reservoir. Thus, the partition coefficients should increase until they reach a maximum at concentrations of ~5% w/w, close to the high-molecular-weight polymer entanglement regime. Any additional polymer concentration increase would result in increasing entanglement, which should result in decreased partition coefficients between the gel and the holes, as observed in Figure 8C.

Conclusions

We have fabricated a periodic array of monodisperse aqueous holes in a hydrogel matrix. We can easily control the size, number density, periodicity, and morphology of these holes. We quantitatively monitored the chemical composition of these holes by probing the refractive index differences between the holes and the medium through Bragg diffraction of the array.

We report here the first direct experimental evidence for the thermodynamic entropic trapping phenomenon. The embedded array of holes serves as entropic traps where flexible polymer chains of NaPSS have the highest conformational freedom and thus can maximize their conformational entropy. As a result, the polymer chains preferentially partition into these holes rather than into the rest of the gel matrix.

Through the Bragg diffraction and absorption spectral studies, we have determined the partition coefficients of linear NaPSS among three regions of different spatial constraints, the monodisperse 100-nm-diameter holes, the random porous hydrogel matrix, and the surrounding reservoir solution. The results show that the NaPSS chains are, indeed, trapped in the space of the least spatial constraints, i.e., the embedded array of holes. The NaPSS concentration in the holes was observed to be ~4-fold higher than that in the gel medium.

We have also systematically investigated the molecular weight and concentration dependence of the partition coefficients. The results are in qualitative agreement with current entropic trapping theory. We suggest that the effective volumes of the hydrogel confining spaces may be molecular weight dependent due to the poorly defined boundary conditions. This diminishes the linear dependence of ln K on polymer molecular weight predicted by entropic trapping theory. We also suggest that the observed concentration dependence of the partition coefficients at high molecular weight may result from the distribution of the pore sizes of the hydrogel.

These mesoscopically periodic HPCCA materials may be useful for applications as novel separation media to separate macromolecules.

Acknowledgment. We gratefully acknowledge Prof. David Pine from the University of California at Santa Barbara and Professor Ana Balasz, John Holtz, Jesse M. Weissman, and Guisheng Pan from the University of Pittsburgh for helpful discussions. We thank the anonymous reviewer who challanged our view of the concentration dependence of the partition coefficients. This work was supported by the Office of Naval Research (Grant N00014-94-1-0592) and the National Science Foundation (Grant CHE-9633561).

JA983843N